JACS
JOURNAL OF THE AMERICAN CHEMICAL SOCIETY
pubs.acs.org/JACS
Communication

Protonation Isomer Specific Ion−Molecule Radical Reactions

Oisin J. Shiels, Samuel J. P. Marlton, and Adam J. Trevitt*

Cite This: J. Am. Chem. Soc. 2023, 145, 15024−15029
Read Online
ACCESS | Metrics & More | Article Recommendations | Supporting Information

ABSTRACT: Through a combination of ion-mobility filtering and laser-equipped quadrupole ion−trap mass spectrometry, the gas-phase reaction kinetics of two protonation isomers of the distonic-radical quinazoline cation are independently measured with ethylene. For these radical addition reactions, protonation site variations drive significant changes in nearby radical reactivity, and this is primarily due to through−space electrostatic effects. Furthermore, quantum chemical methods specifically designed for calculating long-range interactions, such as double-hybrid density functional theory, are required to rationalize the experimentally measured difference in reactivity.

Recent studies have shown that orientated electric fields (OEFs) can catalyze reactions[1−7] and shift electronic excited states[8−10] by (de)stabilizing key transition states.[5,11,12] At the surface of water microdroplets, the electrochemical reduction of organic molecules has been rationalized by high proton concentrations.[13,14] However, since electrostatic effects are highly directional, external OEFs are a challenge to harness for many chemical systems since untethered molecules are typically unaligned in bulk solution. The inclusion of internal charged-moieties in the form of protonated/deprotonated functional groups, hypervalent groups and noncovalently bound ions (e.g., metal ions) can overcome this problem by fixing the position and distance of a charge near/on a molecule.[15] This establishes a fixed internal OEF to be exploited for chemical and photochemical reactivity.

In the case of protonation, the site of protonation on a molecule influences photofragmentation distributions, photoisomerization rates, excited-state lifetimes, and spectroscopic profiles.[16−21] For radical ions, through-space charge effects have been shown to alter the reactivity of gas-phase reactions by several orders of magnitude.[22−24] Additionally, deprotonation can have unexpected consequences on radical reactivity. For example, HOMO-SOMO inversion for deprotonated anion radical ions drastically affects the stability of the radical site.[25,26] Techniques have been developed to generate radical ions with specific OEFs;[27−29] however, there is still much to discover about how OEFs influence the reactivity of radicals. In particular, bespoke experimental methods are needed to accurately measure these effects and benchmark the computational methodology.

Motivated by the need to develop new experimental protocols, this study targets the internal electrostatic effects of an ion-radical pair by measuring the protonation−specific reactions of the 1,3-diazanaphthalene radical cation protomers. First by proving these two protonation isomers can be separated with ion mobility filtering and then probing the reactivity of these species using ion trap kinetics. The electric field at the radical site generated by protonation is significantly different for these two isomers, 215 and 7 A.U., calculated using TITAN;[30] however, these radicals have essentially indistinguishable proton affinities[31] and, as shown below, conventional computational methods are not sufficient to predict the measured relative rates of reaction. The reaction with ethylene is a prototype system for aromatic radical addition to a double bond. Using the combined methods of ion mobility and ion trap mass spectrometry with ion-molecular reactions, we benchmarked the accuracy of several computational methods for predicting the outcomes of these electrostatic effects.

The workflow of this experiment is shown in Figure 1. Brominated diazanaphthalene precursors, dissolved in methanol, are protonated and liberated into the gas-phase by electrospray ionization. The ions pass through field asymmetric ion mobility separation (FAIMS)[32,33] before isolation and storage in an ion trap mass spectrometer. The FAIMS filters and separates the two protonation isomer populations, as confirmed by UVPD action spectroscopy (shown below). After FAIMS selection, a laser pulse induces homolysis of the Br-C bond to generate the 8-dehydroquinazolineH$^+$ distonic radical ion where the protonated site is retained on either the 3-nitrogen or the 1-nitrogen. These distonic radical ions are then stored and allowed to react with ethylene in an ion trap to record the kinetics. For comparison, similar measurements are also reported for 5-dehydroisoquinolinium and 8-dehydroquinolinium, which have unambiguous protonation sites, each analogous to one of the diazanaphthalene protomers (Figure 2).

The FAIMS ionogram of 8-bromoquinazolinium (m/z 209, isotope ^{79}Br) is shown in Figure 3A and contains two broad peaks each centered at compensation voltage (CV) values of −3.5 V and +0.5 V. Quinazoline can be *N*-protonated at the 1-

Received: March 10, 2023
Published: June 20, 2023

https://doi.org/10.1021/jacs.3c02552
J. Am. Chem. Soc. 2023, 145, 15024−15029

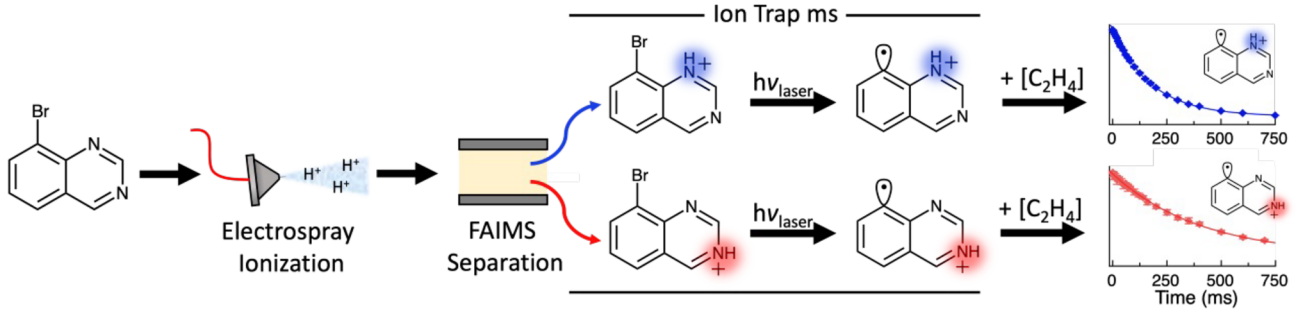

Figure 1. Experimental workflow for protonation-isomer-specific radical reactions.

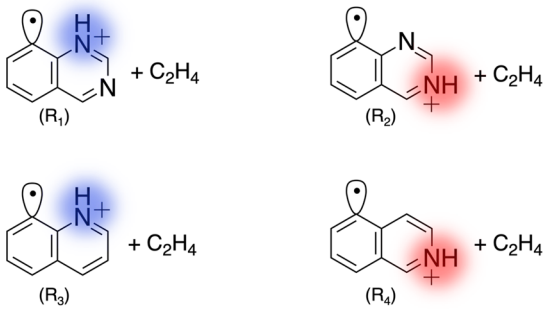

Figure 2. Four reactions targeted in this study. Protonation sites for the two diazanaphthalene reactions, R_1 and R_2, are the same as the 8-dehydroquinolinium and 5-dehydroisoquinolinium reactions R_3 and R_4, respectively (red vs blue highlights).

or 3-nitrogen[31] and these two FAIMS peaks are assigned as the analogous protomers of 8-bromoquinazolinium based on the interpretation of the UVPD action spectra. UVPD of 8-bromoquinazolinium gives rise to photoproducts at m/z 182, 130, 129, 103, and 76. All reported photodissociation action spectra here track the m/z 130 photofragment (arising from ^{79}Br loss).

The action spectrum of ions selected at either FAIMS CV −4 and +1 V are shown in Figure 3B and C, respectively, and there are several broad features over this range. Importantly, the CV −4 V action spectra contains a feature around 420 nm (×200 magnified, labeled I), which is absent in the CV 1 V action spectrum. At higher energies, another feature is observed around 260 nm at CV −4 V (labeled II), which is also absent in the CV +1 V spectrum.

These spectra are compared to Franck−Condon (FC) CAM-B3LYP/aug-cc-pVDZ TD-DFT simulations,[34−36] which have been red-shifted by 2000 cm^{-1}.[37] Features I and II match simulated FC transitions of 3-N protonated 8-dehydroquinazolinium (shaded areas in Figure 3B). These transitions are absent in the FC simulation of the 1-*N* protomer. Based on the absence of these features, as well as the general agreement between the FC simulation and the experimental spectrum, the ion population selected using + 1 V is assigned as the 1-*N* protomer, and the CV −4 V population is assigned to the 3-*N* protomer. However, the presence of a minor population of 1-*N* protonated 8-dehydroquinazolium in Figure 3B cannot be definitively ruled out because feature III overlaps with feature IV in Figure 3C. These assignments are consistent with a previous study on the FAIMS separation of protonated quinazoline, which assigned the lower CV peak as the 3-*N* protonation site and the higher CV peak as 1-*N* protonation.[31]

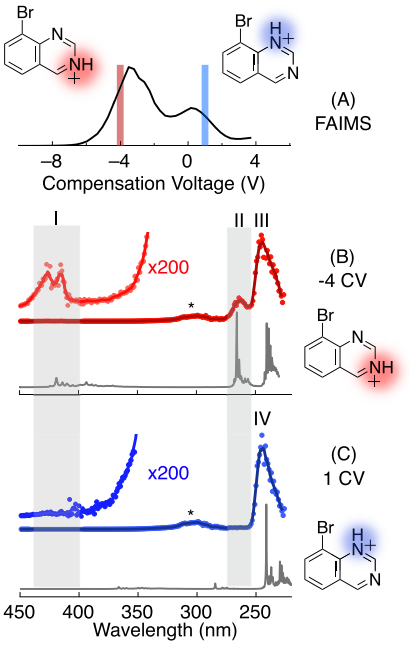

Figure 3. (A) FAIMS ionogram following the m/z 209 signal intensity of protonated 8-bromoquinazoline, using a dispersion voltage of + 5000 V. The peaks at −4 and + 1 V (red and blue bars) are assigned as two protomers of the cation. Photodissociation action spectrum of ions isolated following the yield of m/z 130 photofragment using −4 V (B) and + 1 V (C). The region corresponding to a crystal change of the OPO is denoted with an asterisk (*). Simulated FC transitions of 8-dehydroquinazolinium protonated at the (B) 3-*N* and (C) 1-*N* position using CAM-B3LYP/aug-cc-pVDZ[34−36] (gray line). FC simulations are red-shifted by 2000 cm^{-1}.[37] The shaded areas correspond to features I and II as discussed in the text.

Once introduced into the ion trap and irradiated with a single laser pulse, photodissociation of brominated precursor $[M\text{-}Br]^+$ forms a corresponding radical cation from Br loss (Figure 1). No isomerization is expected following PD due to the high transition state barriers with the available excess energy following C-Br bond homolysis (further details are provided in the Supporting Information). This is further supported by kinetic measurements (*vide infra*).

The target radicals react with ethylene to form adducts $[M + 28]^+$ at either m/z 157 (R_3 and R_4) or m/z 158 (R_1 and R_2). Only R_3 exhibits a prominent H-atom-loss product (m/z 156). Potential energy schemes for these reactions are provided in the Supporting Information. Product mass spectra for each reaction were recorded, and ion signals are plotted as a function of reaction time in Figure 4A−D. These kinetic

https://doi.org/10.1021/jacs.3c02552
J. Am. Chem. Soc. 2023, 145, 15024−15029

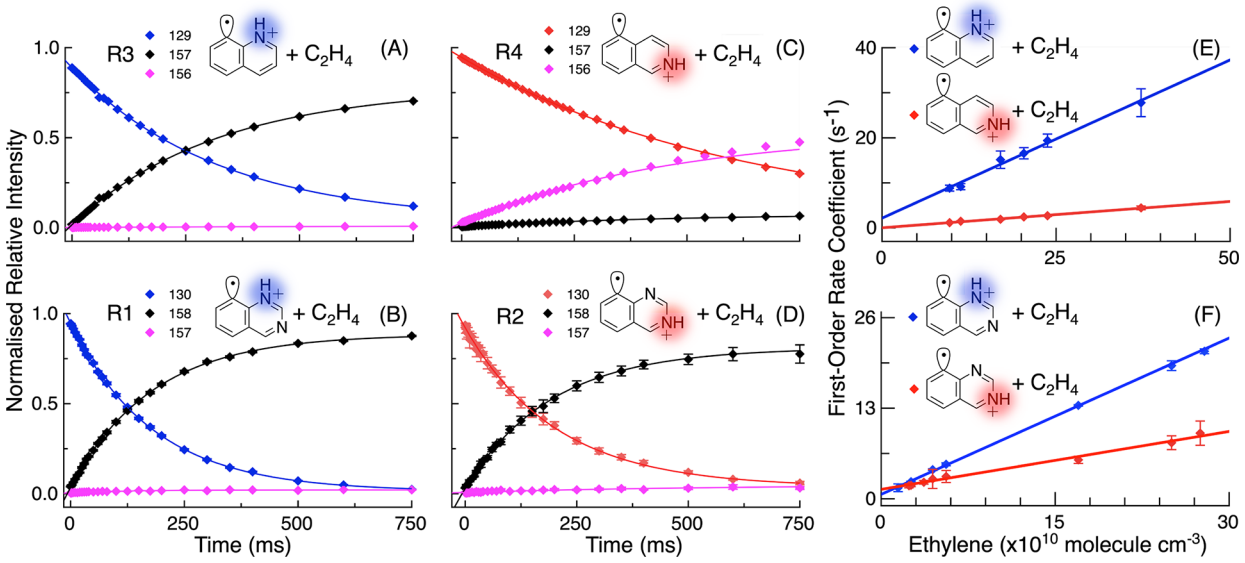

Figure 4. Kinetic profiles for reactions: (A) R3, (B) R1, (C) R4, and (D) R2, where the ethylene concentration is 7.4×10^9 molecule cm^{-3}. First-order reaction coefficient vs ethylene number density, used to extract second-order rate coefficients for (E) R3 and R4 and (F) R1 and R2. Error bars represent 2σ.

Table 1. Experimental Reaction Efficiencies, Second-Order Rate Coefficients, TS_1 Energies (G3X-K and DSD-PBEP86), Adiabatic Electron Affinities (M06-2X), and Hydrogen Bond Energies (M06-2X) for Each Reaction[a]

	R_4	R_3	R_2	R_1
Reaction efficiency (%)	1.4 ± 0.2	8.2 ± 0.7	20 ± 3	42 ± 2
Second-order rate coefficient ($\times 10^{-10}$ cm^3 $molecule^{-1}$ s^{-1})	0.12 ± 0.02	0.70 ± 0.06	1.7 ± 0.3	3.6 ± 0.2
G3X-K transition state energy TS_1 (kJ/mol)	−13 ± 2	−15 ± 2	−19 ± 2	−18 ± 2
DSD-PBEP86 transition state energy TS_1 (kJ/mol)	−13.2 ± 0.4	−14.7 ± 0.4	−18.0 ± 0.4	−20.3 ± 0.4
M06-2X adiabatic electron affinity (eV)	−5.2 ± 0.1	−5.8 ± 0.1	−5.3 ± 0.1	−6.1 ± 0.1
M06-2X hydrogen bond energy (eV)	−12.7 ± 0.1	−12.7 ± 0.1	−12.6 ± 0.1	−12.4 ± 0.1

[a]Uncertainties are the reported RMS errors for each method, when available.[43,44].

experiments were repeated across six ethylene concentrations, and the second-order rate coefficient for each reaction was calculated by plotting *pseudo*-first-order rate coefficients, extracted from these profiles, against the ethylene concentration within the ion trap as discussed in section I of the Supporting Information. These *pseudo*-first-order plots were fitted by linear regression and are plotted in Figure 4E, F. Reaction efficiencies were calculated by normalizing second-order rate coefficients to the Langevin collision rate (ethylene is a neutral molecule with no permanent dipole moment).[38] Branching ratios are given in Table S1 and reaction efficiencies and second-order rate constants are listed in Table 1.

The most efficient reaction is R_1 (42%), followed by R_2 (20%), R_3 (8.2%), and R_4 (1.4%). Importantly, without FAIMS separation, distinct measurements for R_1 and R_2 would not be straightforward. For both quinazoline- and quinoline-based radical cations, the fastest reaction occurs when the proton is closest to the radical site. Additionally, the two quinazoline based radical cations are significantly faster than their quinoline counterparts, indicating that the electron lone pair on the nitrogen accelerates the reaction.

For ion−molecule distonic radical reactions, it is previously observed for 18 different reactions that the energy of the prereactive complex (PRC) has no correlation with the rate of the reaction.[24,39] Instead it is the stability of a long-range PRC transition state that primarily controls the reaction rate. This transition state energy has been used to predict the reactivity of similar distonic radicals, although this parameter is sensitive and requires careful calculation and benchmarking. This means that small changes in the transition state energy will have large impacts on the predicted reaction rate. For the two protonation-isomer reactions, the optimized transition states are shown in Figure 5. Using G3X-K, a high-level composite method,[40] these transition state energies do not align with the

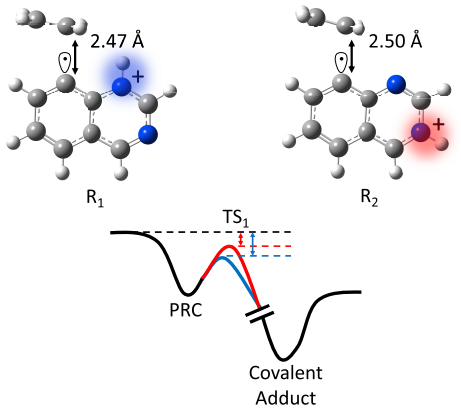

Figure 5. Calculated long-range transition states (TS_1) for R_1 and R_2 (top). A schematic of the reaction surface is also included showing the rate limiting TS_1, between the prereactive complex (PRC) and the covalent adduct, for each reaction in blue and red (bottom).

https://doi.org/10.1021/jacs.3c02552
J. Am. Chem. Soc. 2023, 145, 15024−15029

experimental reaction efficiency trend (Table 1). R_2 has the lowest calculated transition state energy (−19 kJ/mol) and is therefore expected to be the fastest reaction, but the experimental results instead show that R_1 (−18 kJ/mol barrier) has over double the reaction efficiency. This transition state energy difference, however, is within the mean error of this method: ±2 kJ/mol.[41]

To improve the treatment of these transition states each stationary point was recalculated using DSD-PBEP86/aug-cc-pVTZ — a double hybrid method better suited to model long-range electronic effects.[40] Using DSD-PBEP86 the four barrier heights are in the order of the measured reaction efficiency, ascending from R_1 (−20 kJ/mol, 42%) to R_2 (−18 kJ/mol, 20%) to R_3 (−15 kJ/mol, 8.2%) and to R_4 (−13 kJ/mol, 1.4%). The differences in these values lie outside the expected mean error of these calculations (±0.4 kJ/mol)[42] so this interpretation of these results is reasonable. This highlights the importance of double-hybrid methods for systems affected by long-range forces.

Reaction efficiencies of similar ion−molecule reactions have been shown to generally correlate with the electron affinity of the radical cation.[22,45,46] Adiabatic electron affinities for the current systems were calculated using M06-2X/6-31G-(2df,p)[47,48] and are listed in Table 1. Adiabatic electron affinities for a range of other methods are provided in the Supporting Information. However, again, this does not reproduce the ordering of the experiment and serves as a caution for using electron affinities alone as a predictive parameter.

To substantiate the through-space influence on the energy of these rate-limiting transition states, the difference in TS_1 energy between R_1 and R_2 was partitioned into correlation, exchange, and Hartree components (calculated using DSD-PBEP86[40]) following the analysis of Gryn'ova and Coote.[49] These values are summarized in Table 2. For this analysis, a negative value corresponds to a component more stabilized for R_1 and a positive value corresponds to a component more stabilized for R_2. A through-space electrostatic effect will manifest as a difference in the Hartree energy.[49] Thus, the negative Hartree energy (−11 kJ/mol) in Table 2 reveals that the through-space electrostatic interaction is more favorable for R_1 than that for R_2. In contrast, the positive exchange-energy indicates that stabilization *via* electron delocalization is more favorable for R_2, most likely due to the closer range lone-pair interaction with ethylene. The Hartree energy is the dominant component that preferentially stabilizes TS_1 for R_1 and it follows that the increased rate of reaction for R_1 primarily derives from stronger through-space electrostatic stabilization due to the closer protonation site.

Table 2. Difference in Stability between the Rate Limiting Transition State (TS_1) of R_1 and R_2[a]

	Correlation	Exchange	Hartree	Total
(TS_1 R_2) − (TS_1 R_1)	−2	+7	−11	−6

[a]This energy (kJ/mol) is partitioned into the correlation, exchange, and Hartree components.

In summary, these results show that differences in protonation site can dictate nearby radical reactivity, as rationalized by through-space oriented electric field considerations. The experimentally measured rates of reaction are significantly slower (5−20 times) for the quinoline radical cations, indicating that along with the effects of charge location, the nearby electron lone pair on the nitrogen accelerates the reaction for the two quinazoline protomers. These reaction rates correlate to the stability of the calculated long-range prereactive transition state. Importantly, due to the small energy differences between the transition states of these molecules, among the tested methods, only the double hybrid method (DSD-PBEP86) could reproduce the experimental reactivity trend. This method can be applied to any radical−ion reaction if suitable halogenated precursors can be separated with ion filtering techniques.

■ ASSOCIATED CONTENT

Supporting Information

The Supporting Information is available free of charge at https://pubs.acs.org/doi/10.1021/jacs.3c02552.

Experimental details, instrument benchmarking, supporting mass spectra, reaction branching ratios, computational details, potential energy schemes for each reaction (PDF)

■ AUTHOR INFORMATION

Corresponding Author

Adam J. Trevitt − *Molecular Horizons and School of Chemistry and Molecular Bioscience, University of Wollongong, Wollongong 2522 New South Wales, Australia;* orcid.org/0000-0003-2525-3162; Email: adamt@uow.edu.au

Authors

Oisin J. Shiels − *Molecular Horizons and School of Chemistry and Molecular Bioscience, University of Wollongong, Wollongong 2522 New South Wales, Australia*

Samuel J. P. Marlton − *Molecular Horizons and School of Chemistry and Molecular Bioscience, University of Wollongong, Wollongong 2522 New South Wales, Australia;* Present Address: The University of Melbourne, Melbourne 3010, Victoria, Australia

Complete contact information is available at: https://pubs.acs.org/10.1021/jacs.3c02552

Notes

The authors declare no competing financial interest.

■ ACKNOWLEDGMENTS

A.J.T. acknowledge project funding from the Australian Research Council Discovery Program (DP200100065). This work was supported by computational resources provided by the Australian Government through the National Computation Infrastructure under the National Computational Merit Allocation Scheme. O.J.S. and S.J.P.M acknowledge receipt of an Australian Government Research Training Program Scholarship.

■ REFERENCES

(1) Shaik, S; Danovich, D.; Joy, J.; Wang, Z.; Stuyver, T. Electric-field mediated chemistry: Uncovering and exploiting the potential of (oriented) electric fields to exert chemical catalysis and reaction control. *J. Am. Chem. Soc.* **2020**, *142* (29), 12551−62.

(2) Shaik, S.; Ramanan, R.; Danovich, D.; Mandal, D. Structure and reactivity/selectivity control by oriented-external electric fields. *Chem. Soc. Rev.* **2018**, *47* (14), 5125−45.

(3) Stuyver, T.; Danovich, D.; Joy, J.; Shaik, S. External electric field effects on chemical structure and reactivity. Wiley Interdiscip. *Rev. Comput. Mol. Sci.* **2020**, *10* (2), e1438.
(4) Aitken, H. M.; Coote, M. L. Can electrostatic catalysis of Diels−Alder reactions be harnessed with pH-switchable charged functional groups? *Phys. Chem. Chem. Phys.* **2018**, *20* (16), 10671−6.
(5) Ciampi, S.; Darwish, N.; Aitken, H. M.; Díez-Pérez, I.; Coote, M. L. Harnessing electrostatic catalysis in single molecule, electrochemical and chemical systems: a rapidly growing experimental tool box. *Chem. Soc. Rev.* **2018**, *47* (14), 5146−64.
(6) Aragones, A. C.; Haworth, N. L.; Darwish, N.; Ciampi, S.; Bloomfield, N. J.; Wallace, G. G.; Diez-Perez, I.; Coote, M. L. Electrostatic catalysis of a Diels−Alder reaction. *Nature.* **2016**, *531* (7592), 88−91.
(7) Meir, R.; Chen, H.; Lai, W.; Shaik, S. Oriented electric fields accelerate Diels−Alder reactions and control the endo/exo selectivity. *Chem. Phys. Chem.* **2010**, *11* (1), 301−10.
(8) Marlton, S. J. P.; McKinnon, B. I.; Hill, N.; Coote, M. L.; Trevitt, A. J. Electrostatically Tuning the Photodissociation of the Irgacure 2959 Photoinitiator in the Gas Phase by Cation Binding. *J. Am. Soc.* **2021**, *143* (5), 2331−9.
(9) Blyth, M. T.; Noble, B. B.; Russell, I. C.; Coote, M. L. Oriented internal electrostatic fields cooperatively promote ground-and excited-state reactivity: a case study in photochemical CO2 capture. *J. Am. Soc.* **2020**, *142* (1), 606−13.
(10) Hasegawa, J. Y.; Ise, T.; Fujimoto, K. J.; Kikuchi, A.; Fukumura, E.; Miyawaki, A.; Shiro, Y. Excited states of fluorescent proteins, mKO and DsRed: Chromophore− protein electrostatic interaction behind the color variations. *J. Phys. Chem. B.* **2010**, *114* (8), 2971−9.
(11) Zhang, L.; Laborda, E.; Darwish, N.; Noble, B. B.; Tyrell, J. H.; Pluczyk, S.; Le Brun, A. P.; Wallace, G. G.; Gonzalez, J.; Coote, M. L.; Ciampi, S. Electrochemical and electrostatic cleavage of alkoxyamines. *J. Am. Soc.* **2018**, *140* (2), 766−74.
(12) Yu, J. L.; Coote, M. L. Electrostatic switching between SN1 and SN2 pathways. *J. Phys. Chem. A.* **2019**, *123* (2), 582−9.
(13) Lee, J. K.; Samanta, D.; Nam, H. G.; Zare, R. N. Micrometer-sized water droplets induce spontaneous reduction. *J. Am. Soc.* **2019**, *141* (27), 10585−9.
(14) Ruiz-Lopez, M. F.; Francisco, J. S.; Martins-Costa, M. T.; Anglada, J. M. Molecular reactions at aqueous interfaces. *Nature Reviews Chemistry.* **2020**, *4* (9), 459−75.
(15) Hill, N. S.; Coote, M. L. Internal oriented electric fields as a strategy for selectively modifying photochemical reactivity. *J. Am. Soc.* **2018**, *140* (50), 17800−4.
(16) Matthews, E.; Dessent, C. E. Experiment and theory confirm that UV laser photodissociation spectroscopy can distinguish protomers formed via electrospray. *Phys. Chem. Chem. Phys.* **2017**, *19* (26), 17434−40.
(17) Bull, J. N.; Coughlan, N. J.; Bieske, E. J. Protomer-Specific Photochemistry Investigated Using Ion Mobility Mass Spectrometry. *J. Phys. Chem. A.,* **2017**, *121* (32), 6021−7.
(18) Matthews, E.; Cercola, R.; Dessent, C. E. Protomer-dependent electronic spectroscopy and photochemistry of the model flavin chromophore alloxazine. *Molecules.,* **2018**, *23* (8), 2036.
(19) Wysocki, V. H.; Tsaprailis, G.; Smith, L. L.; Breci, L. A. Mobile and localized protons: a framework for understanding peptide dissociation. *Mass Spectrom.* **2000**, *35* (12), 1399−406.
(20) Marlton, S. J. P.; McKinnon, B. I.; Ucur, B.; Maccarone, A. T.; Donald, W. A.; Blanksby, S. J.; Trevitt, A. J. Selecting and identifying gas-phase protonation isomers of nicotineH+ using combined laser, ion mobility and mass spectrometry techniques. *Faraday Discuss.* **2019**, *217*, 453−475.
(21) Xia, H.; Attygalle, A. B. Transformation of the gas-phase favored O-protomer of p-aminobenzoic acid to its unfavored N-protomer by ion activation in the presence of water vapor: A n ion-mobility mass spectrometry study. *J. Mass Spectrom.* **2018**, *53* (4), 353−60.
(22) Shiels, O. J.; Kelly, P. D.; Bright, C. C.; Poad, B. L. J.; Blanksby, S. J.; da Silva, G.; Trevitt, A. J. Reactivity Trends in the Gas-Phase Addition of Acetylene to the N-Protonated Aryl Radical Cations of Pyridine, Aniline, and Benzonitrile. *J. Am. Soc. Mass Spectrom.* **2021**, *32* (2), 537−47.
(23) Shiels, O. J.; Kelly, P. D.; Blanksby, S. J.; da Silva, G.; Trevitt, A. J. Barrierless Reactions of Three Benzonitrile Radical Cations with Ethylene. *Aust. J. Chem.* **2020**, *73* (8), 705−13.
(24) Shiels, O. J; Turner, J. A.; Kelly, P. D.; Blanksby, S. J.; da Silva, G.; Trevitt, A. J Modelling reaction kinetics of distonic radical ions: a systematic investigation of phenyl-type radical addition to unsaturated hydrocarbons. *Faraday Discuss.* **2022**, *238*, 475−90.
(25) Kumar, A.; Sevilla, M. D. SOMO−HOMO Level Inversion in Biologically Important Radicals. *J. Phys. Chem. B.* **2018**, *122* (1), 98−105.
(26) Kumar, A.; Sevilla, M. D. Proton transfer induced SOMO-to-HOMO level switching in one-electron oxidized AT and GC base pairs: A density functional theory study. *J. Phys. Chem. B.* **2014**, *118* (20), 5453−8.
(27) Chyall, L. J.; Kenttamaa, H. I. The 4-dehydroanilinium ion: a stable distonic isomer of ionized aniline. *J. Am. Soc.* **1994**, *116* (7), 3135−6.
(28) Reed, D. R.; Hare, M. C.; Fattahi, A.; Chung, G.; Gordon, M. S.; Kass, S. R. α, 2-, α, 3-, and α, 4-Dehydrophenol Radical Anions: Formation, Reactivity, and Energetics Leading to the Heats of Formation of α, 2-, α, 3-, and α, 4-Oxocyclohexadienylidene. *J. Am. Soc.* **2003**, *125* (15), 4643−51.
(29) Wenthold, P. G.; Hu, J.; Squires, R. R. o-, m-, and p-benzyne negative ions in the gas phase: Synthesis, authentication, and thermochemistry. *J. Am. Soc.* **1996**, *118* (47), 11865−71.
(30) Stuyver, T.; Huang, J.; Mallick, D.; Danovich, D.; Shaik, S. TITAN: A code for modeling and generating electric fields—features and applications to enzymatic reactivity. *J. Comput. Chem.* **2020**, *41* (1), 74−82.
(31) Marlton, S. J. P.; McKinnon, B. I.; Ucur, B.; Bezzina, J. P.; Blanksby, S. J.; Trevitt, A. J. Discrimination between protonation isomers of quinazoline by ion mobility and uv-photodissociation action spectroscopy. *J. Phys. Chem. Lett.* **2020**, *11* (10), 4226−31.
(32) Shvartsburg, A. A. *Differential Ion Mobility Spectrometry: Nonlinear Ion Transport, and Fundamentals of FAIMS;* CRC Press, 2008.
(33) Guevremont, R. High-field asymmetric waveform ion mobility spectrometry: a new tool for mass spectrometry. *Journal of Chromatography A.* **2004**, *1058* (1−2), 3−19.
(34) Yanai, T.; Tew, D. P.; Handy, N. C. A new hybrid exchange−correlation functional using the Coulomb-attenuating method (CAM-B3LYP). *Chem. Phys. Lett.* **2004**, *393* (1), 51−57.
(35) Dunning, T. H., Jr Gaussian basis sets for use in correlated molecular calculations. I. The atoms boron through neon and hydrogen. *The Journal of chemical physics* **1989**, *90* (2), 1007−1023.
(36) Woon, D. E.; Dunning, T. H., Jr Gaussian basis sets for use in correlated molecular calculations. III. The atoms aluminum through argon. *The Journal of chemical physics* **1993**, *98* (2), 1358−1371.
(37) Kulesza, A. J.; Titov, E.; Daly, S.; Włodarczyk, R.; Megow, J.; Saalfrank, P.; Choi, C. M.; MacAleese, L.; Antoine, R.; Dugourd, P. Excited States of Xanthene Analogues: Photofragmentation and Calculations by CC2 and Time-Dependent Density Functional Theory. *ChemPhysChem.* **2016**, *17* (19), 3129−38.
(38) Langevin, M. P. Une formule fondamentale de théorie cinétique. *Annales de chimie et de physique* **1905**, *5*, 245−288.
(39) Bright, C. C.; Prendergast, M. B.; Kelly, P. D.; Bezzina, J. P.; Blanksby, S. J.; da Silva, G.; Trevitt, A. J. Highly efficient gas-phase reactivity of protonated pyridine radicals with propene. *Phys. Chem. Chem. Phys.* **2017**, *19* (46), 31072−84.
(40) da Silva, G. G3X-K theory: A composite theoretical method for thermochemical kinetics. *Chem. Phys. Lett.* **2013**, *558*, 109−13.
(41) Kozuch, S.; Martin, J. M. L. DSD-PBEP86: in search of the best double-hybrid DFT with spin-component scaled MP2 and dispersion corrections. *Phys. Chem. Chem. Phys.* **2011**, *13* (45), 20104−7.
(42) Yu, F.; Fu, L. X.; Yang, Y. DSD-PBEP86-NL and DOD-PBEP86-NL functionals for noncovalent interactions: Basis set effects

https://doi.org/10.1021/jacs.3c02552
J. Am. Chem. Soc. 2023, 145, 15024−15029

and tentative applications to large noncovalent systems. *Int. J. Quantum Chem.* **2017**, *117* (19), e25417.
(43) Su, N. Q.; Zhang, I. Y.; Wu, J.; Xu, X. Calculations of ionization energies and electron affinities for atoms and molecules: A comparative study with different methods. *Frontiers of Chemistry in China.* **2011**, *6* (4), 269−279.
(44) Goerigk, L.; Hansen, A.; Bauer, C.; Ehrlich, S.; Najibi, A.; Grimme, S. A look at the density functional theory zoo with the advanced GMTKN55 database for general main group thermochemistry, kinetics and noncovalent interactions. *Phys. Chem. Chem. Phys.* **2017**, *19* (48), 32184−215.
(45) Petzold, C. J.; Nelson, E. D.; Lardin, H. A.; Kenttämaa, H. I. Charge-site effects on the radical reactivity of distonic ions. *J. Phys. Chem. A.* **2002**, *106* (42), 9767−75.
(46) Williams, P. E.; Jankiewicz, B. J.; Yang, L.; Kenttämaa, H. I. Properties and reactivity of gaseous distonic radical ions with aryl radical sites. *Chem. Rev.,* **2013**, *113* (9), 6949−85.
(47) Zhao, Y.; Truhlar, D. G. The M06 suite of density functionals for main group thermochemistry, thermochemical kinetics, noncovalent interactions, excited states, and transition elements: two new functionals and systematic testing of four M06-class functionals and 12 other functionals. *Theoretical chemistry accounts.* **2008**, *120* (1), 215−41.
(48) Frisch, M. J.; Pople, J. A.; Binkley, J. S. Self-consistent molecular orbital methods 25. Supplementary functions for Gaussian basis sets. *The Journal of chemical physics.* **1984**, *80* (7), 3265−9.
(49) Gryn'ova, G.; Coote, M. L Directionality and the role of polarization in electric field effects on radical stability. *Aust. J. Chem.* **2017**, *70* (4), 367−72.

https://doi.org/10.1021/jacs.3c02552
J. Am. Chem. Soc. 2023, 145, 15024−15029